IV International Conference on Computational Methods for Coupled Problems in Science and Engineering
COUPLED PROBLEMS 2011
M. Papadrakakis, E. Oñate and B. Schrefler (Eds)

IMMERSED BOUNDARY METHOD: PERFORMANCE ANALYSIS OF POPULAR FINITE ELEMENT SPACES

DANIELE BOFFI*, NICOLA CAVALLINI*, FRANCESCA GARDINI* AND LUCIA GASTALDI†

*Dipartimento di Matematica "F. Casorati"
Università di Pavia
Via Ferrata 1, 27100 Pavia, Italy
{daniele.boffi,nicola.cavallini,francesca.gardini}@unipv.it

†Dipartimento di Matematica
Università di Brescia,
via Valotti, 9 - 25133, Brescia, Italy,
lucia.gastaldi@ing.unibs.it

Key words: Finite Elements, Immersed Boundary Method, Fluid-Structure Interactions, Mass conservation.

Abstract. The aim of this paper is to understand the performances of different finite elements in the space discretization of the Finite Element Immersed Boundary Method. In this exploration we will analyze two popular solution spaces: *Hood-Taylor* and *Bercovier-Pironneau* (P1-iso-P2). Immersed boundary solution is characterized by pressure discontinuities at fluid structure interface. Due to such a discontinuity a natural enrichment choice is to add piecewise constant functions to the pressure space. Results show that $P_1 + P_0$ pressure spaces are a significant cure for the well known "boundary leakage" affecting IBM. Convergence analysis is performed, showing how the discontinuity in the pressure is affecting the convergence rate for our finite element approximation.

1 INTRODUCTION

Several applications involve the dynamical interaction of solids and fluids. Compatibility and dynamical conditions are set to quantify the mechanical phenomenology involving the solid and fluid phases. Solid equations are naturally written in a Lagrangian framework, fluid equations are written in an Eulerian framework. The duality between Lagrangian and Eulerian coordinates is the first issue regarding fluid-structure interactions.

There are different strategies for the coupling of Lagrangian and Eulerian descriptions. Among those we recalll the Arbitrary Lagrangian Eulerian approach [13, 14, 12, 15] and

the fictitious domain method [8, Ch. 8].

The subject of this paper is the immersed boundary method (IBM). The IBM was first introduced by Peskin in the 70's in order to simulate the heart blood flow during a cardiac beat. In the case of immersed boundary method the structure is fully immersed in the fluid. We refer to [16] for a review of the method. The main idea is to consider the structure as a part of the fluid. At the fluid and solid overlap, the resulting stress tensor and density consist of a combination of the fluid and solid ones. In this manner fluid and solid can be treated in their natural formulation, Eulerian and Lagrangian respectively. In its original finite difference formulation the IBM takes into account fluid-solid interface conditions by means of a Dirac delta function. The finite difference approximation of Dirac delta functions is characterized by an intrinsically diffusive behavior. A great effort is produced to stabilize this effect and to minimize the well know "boundary leakage" phenomena [10, 11, 9].

Recently, a finite element approximation of the IBM has been introduced [3, 6, 5, 7, 2]. The finite element discretization of IBM treats variationally the interface between the fluid and the solid, resulting in a natural embedding of the solid equations into the fluid ones. The variational treatment of the discontinuity results in a sharper separation of fluid and solid, see [3, 4].

In this paper we explore the performances related to different popular solution spaces for the Navier-Stokes equations solution. We start analyzing the *Bercovier–Pironneau* (P1-iso-P2) and the *Hood–Taylor* finite elements. Then we take advantage of the variational treatment of the fluid solid interface, and we add piecewise constant functions to the pressure space. In this way we give a variational interpretation of the discontinuity between fluid and solid. Adding a P_0 to the pressure solution space results in a five times reduced "boundary leakage". Moreover the oscillations due to the approximation of discontinuous solution with continuous pressure functions are reduced. On the other hand we will show that the solution spaces for the velocities are characterized by non intuitive behavior. The *Hood–Taylor* element is more accurate than the *Bercovier–Pironneau*, but the resulting diffusivity is higher.

This paper is organized as follows. In Section 2 we recall the formulation of our problem, in Section 3 we recall the discrete formulation of our problem, Section 4 is dedicated to the numerical experiments. Careful attention will be paid to the results of choices in Section 3.1. Finally in Section 5 we draw our conclusions.

2 PROBLEM FORMULATION

Let $\Omega \subset \mathbb{R}^d$, $d = 2, 3$, be a region containing a fluid and an immersed solid material. In particular, we focus on viscous incompressible fluids and incompressible viscoelastic structures. The natural framework for the fluid dynamics is Eulerian, the solid mechanics is usually described using Lagrangian coordinates. The key feature of the IB is assuming that the stress tensor at the overlapping between fluid and solid equals the sum of the fluid and structure stress tensors. In this way fluid and structure can be properly treated

in their natural framework.

At time t the solid body is located in $\mathcal{B}_t \subset \Omega$, which is the image of a reference domain $\mathcal{B} \subset \mathbb{R}^m$, $m = d, d-1$, through a mapping $\mathbf{X}$. We set up our Lagrangian framework denoting $\mathbf{s}$ the variable in the reference domain $\mathcal{B}$ and $\mathbf{x}$ as a material point in the current domain $\mathcal{B}_t$. Moreover, we assume that $\partial\mathcal{B}_t \cap \partial\Omega = \emptyset$. From now on we consider the reference domain coinciding with the initial domain, that is $\mathcal{B} = \mathcal{B}_0$.

The relationship between the two different frameworks is given by the mapping

$$\mathbf{X} : \mathcal{B} \times [0,T] \to \mathcal{B}_t \quad \text{so that } \mathbf{x} = \mathbf{X}(\mathbf{s},t)\ \forall \mathbf{x} \in \mathcal{B}_t. \tag{1}$$

We assume that at any given time the mapping $\mathbf{X}(\mathbf{s},t)$ is invertible, which implies that the deformation gradient

$$\mathbb{F}_{\alpha i} := \big(\boldsymbol{\nabla}_s \mathbf{X}(\mathbf{s},t)\big)_{\alpha i} = \mathbf{X}_{\alpha,i}(\mathbf{s},t) = \frac{\partial \mathbf{X}_\alpha(\mathbf{s},t)}{\partial s_i}, \tag{2}$$

has rank m. We assume that the quantity $|\mathbb{F}|$ defined as

$$|\mathbb{F}| = \begin{cases} \left|\dfrac{\partial \mathbf{X}}{\partial s}\right| & \text{if } m = 1 \\ \left|\dfrac{\partial \mathbf{X}}{\partial s_1} \wedge \dfrac{\partial \mathbf{X}}{\partial s_2}\right| & \text{if } m = 2 \\ \left|\left(\dfrac{\partial \mathbf{X}}{\partial s_1} \wedge \dfrac{\partial \mathbf{X}}{\partial s_2}\right) \cdot \dfrac{\partial \mathbf{X}}{\partial s_3}\right| & \text{if } m = 3, \end{cases} \tag{3}$$

is positive at time $t = 0$, and therefore at any subsequent time.

Velocity and acceleration of a particle at $\mathbf{x}$ at time t are respectively defined as:

$$\mathbf{u}(\mathbf{x},t) = \frac{\partial \mathbf{X}}{\partial t}(\mathbf{s},t) \quad \text{for } \mathbf{x} = \mathbf{X}(\mathbf{s},t), \tag{4}$$

and

$$\dot{\mathbf{u}}(\mathbf{x},t) = \frac{D\mathbf{u}}{dt}(\mathbf{x},t) = \frac{\partial^2 \mathbf{X}}{\partial t^2}(\mathbf{s},t) = \frac{\partial \mathbf{u}}{\partial t}(\mathbf{x},t) + \mathbf{u}(\mathbf{x},t) \cdot \boldsymbol{\nabla}\, \mathbf{u}(\mathbf{x},t), \tag{5}$$

We assume homogeneous and incompressible fluid and solid, so that the density ρ is piecewise constant:

$$\rho = \begin{cases} \rho_f & \text{in } \Omega \setminus \mathcal{B}_t \\ \rho_s & \text{in } \mathcal{B}_t. \end{cases} \tag{6}$$

Detailed study of stability criteria regarding the ratio ρ_s/ρ_f can be found in [2].

The Cauchy stress tensor $\boldsymbol{\sigma}$, is considered equal to the fluid one, where no solid phase is located. Where the fluid and the solid overlap the fluid and the solid stresses are summed:

$$\boldsymbol{\sigma} = \begin{cases} \boldsymbol{\sigma}_f & \text{in} \quad \Omega \backslash \mathcal{B}_t \\ \boldsymbol{\sigma}_f + \boldsymbol{\sigma}_s & \text{in} \quad \mathcal{B}_t \end{cases} \tag{7}$$

This assumption is satisfied for example by some biological tissues, subject of several fluid structure interaction problems (see, e.g., [18]). The fluid stress tensor is specified for viscous fluids of type:

$$\boldsymbol{\sigma}_f = -p\mathbb{I} + \mu(\nabla \mathbf{u} + (\nabla \mathbf{u})^T) \tag{8}$$

The solid stress tensor $\boldsymbol{\sigma}_s$ is expressed in Lagrangian variables by means of the first Piola-Kirchhoff stress tensor $\mathbb{P}$:

$$\mathbb{P}(\mathbf{s},t) = |\mathbb{F}(\mathbf{s},t)|\, \boldsymbol{\sigma}_s(\mathbf{X}(\mathbf{s},t),t)\, \mathbb{F}^{-T}(\mathbf{s},t). \tag{9}$$

The previous definitions are combined with the principal of virtual work, the balance of momenta and $|\mathbb{F}| = 1$ to get:

$$\int_\Omega (\rho_f \dot{\mathbf{u}} - \boldsymbol{\nabla}\cdot\boldsymbol{\sigma}_f)\cdot\mathbf{v}\mathrm{d}\mathbf{x} = -(\rho_s-\rho_f)\int_{\mathcal{B}} \frac{\partial^2 \mathbf{X}}{\partial t^2}\cdot\mathbf{V}\mathrm{d}\mathbf{s} + \int_{\mathcal{B}} (\nabla_s\cdot\mathbb{P})\cdot\mathbf{V}\mathrm{d}\mathbf{s} - \int_{\partial\mathcal{B}} \mathbb{P}\mathbf{N}\cdot\mathbf{V}\mathrm{d}\mathrm{A}. \tag{10}$$

where $\mathbf{V}(\mathbf{s},t) = \mathbf{v}(\mathbf{X}(\mathbf{s},t))$, and $\mathbf{N}$ is the outer normal to the region $\mathcal{B}$ in Lagrangian coordinates. The change of variables between Eulerian and Lagrangian can be avoided using the defining property of the d-dimensional Dirac delta distribution:

$$\mathbf{V}(\mathbf{s},t) = \mathbf{v}(\mathbf{X}(\mathbf{s},t)) = \int_\Omega \mathbf{v}(\mathbf{x})\boldsymbol{\delta}(\mathbf{x}-\mathbf{X}(\mathbf{s},t))\mathrm{d}\mathbf{x} \quad \forall \mathbf{s}\in\mathcal{B}. \tag{11}$$

Taking into account the definition of $\boldsymbol{\sigma}_f$ and noticing that $\mathbf{v}$ is arbitrary we conclude the derivation of our problem: find $\mathbf{u}$, p and $\mathbf{X}$ which satisfy the Navier–Stokes equations

$$\rho_f\left(\frac{\partial \mathbf{u}}{\partial t} + \mathbf{u}\cdot\nabla\mathbf{u}\right) - \mu\Delta\mathbf{u} + \nabla p = \mathbf{d}+\mathbf{f}+\mathbf{t} \quad \text{in } \Omega\times]0,T[\tag{12}$$

$$\nabla\cdot\mathbf{u} = 0 \quad \text{in } \Omega\times]0,T[\tag{13}$$

with the following source terms

$$\mathbf{d}(\mathbf{x},t) = -(\rho_s-\rho_f)\int_{\mathcal{B}} \frac{\partial^2\mathbf{X}}{\partial t^2}\boldsymbol{\delta}(\mathbf{x}-\mathbf{X}(\mathbf{s},t))\mathrm{d}\mathbf{s} \quad \text{in } \Omega\times]0,T[\tag{14}$$

$$\mathbf{f}(\mathbf{x},t) = \int_{\mathcal{B}} \nabla_s\cdot\mathbb{P}\boldsymbol{\delta}(\mathbf{x}-\mathbf{X}(\mathbf{s},t))\mathrm{d}\mathbf{s} \quad \text{in } \Omega\times]0,T[\tag{15}$$

$$\mathbf{t}(\mathbf{x},t) = -\int_{\partial\mathcal{B}} \mathbb{P}\mathbf{N}\boldsymbol{\delta}(\mathbf{x}-\mathbf{X}(\mathbf{s},t))\mathrm{d}\mathrm{A} \quad \text{in } \Omega\times]0,T[\tag{16}$$

and the following equation for the immersed boundary with suitable boundary and initial conditions

$$\frac{\partial\mathbf{X}}{\partial t}(\mathbf{s},t) = \mathbf{u}(\mathbf{X}(\mathbf{s},t),t) \quad \text{in } \mathcal{B}\times]0,T[\tag{17}$$

$$\mathbf{u}(\mathbf{x},t) = 0 \quad \text{on } \partial\Omega\times]0,T[\tag{18}$$

$$\mathbf{u}(\mathbf{x},0) = \mathbf{u}_0(\mathbf{x}) \quad \text{in } \Omega \tag{19}$$

$$\mathbf{X}(\mathbf{s},0) = \mathbf{X}_0(\mathbf{s}) \quad \text{in } \mathcal{B}. \tag{20}$$

3 FINITE ELEMENT DISCRETIZATION

We now recall how to discretize the problem using finite element in space and a semi-implicit approach in time. We refer to [2] for more details.

Let $\mathcal{T}_h$ be a subdivision of Ω into triangles or rectangles if $d = 2$, tetrahedrons or parallelepipeds if $d = 3$, being K a single element of $\mathcal{T}_h$. We consider two finite dimensional spaces $V_h \subseteq H_0^1(\Omega)^d$ and $Q_h \subseteq L_0^2(\Omega)$.

Next consider a subdivision $\mathcal{S}_h$ of $\mathcal{B}$ into segments, triangles or tetrahedrons for $m = 1, 2, 3$ respectively. We shall use the following notation: T_k, $k = 1, \dots, M_e$ denotes an element of $\mathcal{S}_h$, $\mathbf{s}_j$, $j = 1, \dots, M$ stands for a vertex of $\mathcal{S}_h$, and $\mathcal{E}_h$ indicates the set of the edges (or faces) e of $\mathcal{S}_h$. Then S_h is the finite element space of piecewise linear d-vectors defined on $\mathcal{B}$ as follows

$$S_h = \{\mathbf{Y} \in C^0(\mathcal{B}; \Omega) : \quad \mathbf{Y}|_{T_k} \in P_1(T_k)^d, \ k = 1, \dots, M_e\}, \tag{21}$$

where $P_1(T_k)$ stands for the space of affine polynomials on the element T_k. For an element $\mathbf{Y} \in S_h$ we shall use also the following notation $\mathbf{Y}_j = \mathbf{Y}(\mathbf{s}_j)$ for $j = 1, \dots, M$.

One of the crucial points of our method is the evaluation of the force term. We consider $\mathbf{X}_h$ piecewise linear so that the deformation gradient $\mathbb{F}_h = \boldsymbol{\nabla}_s \mathbf{X}_h$ is piecewise constant. Therefore also $\mathbb{P}_h = \mathbb{P}(\mathbb{F}_h)$ is piecewise constant and we can work as follows for all $\mathbf{v} \in V_h$:

$$\begin{aligned} \langle \mathbf{F}_h(t), \mathbf{v} \rangle &= -\sum_{k=1}^{M_e} \int_{T_k} \mathbb{P}_h|_{T_k} : \nabla_s \mathbf{v}(\mathbf{X}_h) \, \mathrm{d}\mathbf{s} \\ &= -\sum_{k=1}^{M_e} \int_{\partial T_k} \mathbb{P}_h|_{T_k} \mathbf{N} \cdot \mathbf{v}(\mathbf{X}_h) \mathrm{dA} \\ &= -\sum_{e \in \mathcal{E}_h} \int_e [\![\mathbb{P}_h]\!] \cdot \mathbf{v}(\mathbf{X}_h) \mathrm{dA} \end{aligned} \tag{22}$$

where $[\![\mathbb{P}_h]\!]$ is the jump of $\mathbb{P}_h$ across the interelement edge e, defined as:

$$[\![\mathbb{P}_h]\!] = \mathbb{P}_h^+ \mathbf{N}^+ + \mathbb{P}_h^- \mathbf{N}^-, \tag{23}$$

and $\mathbf{N}^+$ and $\mathbf{N}^-$ are the normals to the interface e pointing outward "+" or inward "−" the element. Moreover we use the convention that, when $e \in \partial\mathcal{B}$, then $[\![\mathbb{P}_h]\!] = \mathbb{P}_h \mathbf{N}$, where $\mathbf{N}$ is the outer normal to $\mathcal{B}$. We observe that e could be either a face (if $m = 3$) or an edge (if $m = 2$) or a point (if $m = 1$). In the first two cases the integrals are computed with a suitable quadrature formula, while in the latter case there are no integrals in the formula. Moreover, the computation of (22) requires an interpolation procedure in order to evaluate the test function along the structure.

3.1 Stable Finite Elements

In this work we focus on two popular finite elements in two dimensions: *Bercovier–Pironneau* (P1-isoP2) and *Hood–Taylor*. In the IB method the structure imposes a discontinuity in the solution for the stress while the velocity is still continuous. This is the reason why we add piecewise constant functions to the pressure space for both elements.

The numerical experiments will compare *Hood–Taylor* finite element:

$$\begin{aligned} V_h &= \{\mathbf{v} \in H_0^1(\Omega)^2 : \mathbf{v}|_K \in P_2(K)^2 \ \forall K \in \mathcal{T}_h\}, \\ Q_h &= \{q \in L_0^2(\Omega) : q = q_1,\ q_1 \in C(\bar{\Omega}),\ q_1|_K \in P_1(K)\ \forall K \in \mathcal{T}_h\}, \end{aligned} \tag{24}$$

and its augmented version:

$$\begin{aligned} V_h &= \{\mathbf{v} \in H_0^1(\Omega)^2 : \mathbf{v}|_K \in P_2(K)^2 \ \forall K \in \mathcal{T}_h\}, \\ Q_h &= \{q \in L_0^2(\Omega) : q = q_1 + q_0,\ q_1 \in C(\bar{\Omega}),\ q_1|_K \in P_1(K),\ q_0|_K \in P_0(K)\ \forall K \in \mathcal{T}_h\}. \end{aligned} \tag{25}$$

The *Bercovier–Pironneau* will be also tested:

$$\begin{aligned} V_h &= \{\mathbf{v} \in H_0^1(\Omega)^2 : \mathbf{v}|_K \in P_1(K)^2 \ \forall K \in \mathcal{T}_{h/2}\}, \\ Q_h &= \{q \in L_0^2(\Omega) : q = q_1,\ q_1 \in C(\bar{\Omega}),\ q_1|_K \in P_1(K)\ \forall K \in \mathcal{T}_h\}, \end{aligned} \tag{26}$$

and its augmented version will be considered as well:

$$\begin{aligned} V_h &= \{\mathbf{v} \in H_0^1(\Omega)^2 : \mathbf{v}|_K \in P_1(K)^2 \ \forall K \in \mathcal{T}_{h/2}\}, \\ Q_h &= \{q \in L_0^2(\Omega) : q = q_1 + q_0,\ q_1 \in C(\bar{\Omega}),\ q_1|_K \in P_1(K),\ q_0 \in P_0(K)\ \forall K \in \mathcal{T}_h\}, \end{aligned} \tag{27}$$

here $\mathcal{T}_{h/2}$ is the mesh obtained connecting the midpoints of every element of $\mathcal{T}_h$. In [1] we used the macroelement technique to prove that the inf-sup condition, for the Stokes problem, is satisfied for the augmented finite elements (see also [17, 19]). Introducing the augmented pressure space for the Stokes problem we reduced the difference between analytical and numerical solution. Moreover the *Hood–Taylor* confirmed a more accurate behaviour with respect to *Bercovier–Pironneau*.

In the case of IB we expect two significant improvements in the elements performances:

1. A better mass conservation. Considering a $P_1 + P_0$ test function for the pressure is equivalent to impose the subsequent restriction:

$$\int_K \nabla \cdot \mathbf{u} \, \mathrm{d}\mathbf{x} = 0 \tag{28}$$

   being K a generic triangle in $\mathcal{T}_h$.

2. We expect a sharper profile in the pressure solution. The original formulation of *Bercovier–Pironneau* and *Hood–Taylor* approximate the pressure with continuous functions. This causes a Gibbs phenomenon at pressure discontinuity. We expect $P_1 + P_0$ functions to better control this Gibbs phenomenon.

The second order derivative of $\mathbf{X}_h$ with respect to time is discretized with the usual second order finite difference and then approximated using the discrete counterpart of (17). Hence the scheme reads as follows:

Step 1. Compute

$$\langle \mathbf{F}_h^{n+1}, \mathbf{v} \rangle = -\sum_{e \in \mathcal{E}_h} [\![\mathbb{P}_h]\!]^n \cdot \mathbf{v}(\mathbf{X}_h^n(s,t)) \, \mathrm{dA} \qquad \forall \mathbf{v} \in V_h. \tag{29}$$

Step 2. Solve the Navier-Stokes equations: find $(\mathbf{u}_h^{n+1}, p_h^{n+1}) \in V_h \times Q_h$ such that

$$\begin{aligned} &\rho_f \left(\frac{\mathbf{u}_h^{n+1} - \mathbf{u}_h^n}{\Delta t}, \mathbf{v} \right) + b(\mathbf{u}_h^{n+1}, \mathbf{u}_h^{n+1}, \mathbf{v}) + a(\mathbf{u}_h^{n+1}, \mathbf{v}) - (\boldsymbol{\nabla} \cdot \mathbf{v}, p_h^{n+1}) = \\ &\quad - (\rho_s - \rho_f) \int_{\mathcal{B}} \frac{\mathbf{u}_h^{n+1}(\mathbf{X}_h^n(s)) - \mathbf{u}_h^n(\mathbf{X}_h^{n-1}(s))}{\Delta t} \cdot \mathbf{v}(\mathbf{X}_h^n(s)) \mathrm{d}\mathbf{s} + \langle \mathbf{F}_h^{n+1}, \mathbf{v} \rangle \quad \forall \mathbf{v} \in V_h \\ &(\boldsymbol{\nabla} \cdot \mathbf{u}_h^{n+1}, q) = 0 \qquad \forall q \in Q_h. \end{aligned} \tag{30}$$

Step 3. Advance the position of the points of the structure:

$$\frac{\mathbf{X}_{hi}^{n+1} - \mathbf{X}_{hi}^n}{\Delta t} = \mathbf{u}_h^{n+1}(\mathbf{X}_{hi}^n) \quad \forall i = 1, \ldots, M. \tag{31}$$

4 NUMERICAL EXPERIMENTS

This section is devoted to numerical experiments. We refer to the popular inflated balloon test case. We are considering a two-dimensional domain, the square $[0,1]^2$, for a Stokes fluid. The immersed boundary is lying along a circle of radius $R = 0.4$. The immersed boundary initial parametric representation is:

$$\mathbf{X}_0(s) = \begin{pmatrix} R\cos(s/R) + 0.5 \\ R\sin(s/R) + 0.5 \end{pmatrix}, \quad s \in [0, 2\pi R] \, .$$

The elastic distributed load is written as follows:

$$\langle \mathbf{F}(t), \mathbf{v} \rangle = -\kappa \int_0^{2\pi R} \frac{\partial \mathbf{X}(s,t)}{\partial s} \frac{\partial \mathbf{v}(\mathbf{X}(s,t))}{\partial s}. \tag{32}$$

where κ represents the structure stiffness.

This parametric representation of the immersed boundary, together with the tension formulation in (32), results in a distributed load per unit length equal to κ/R, radially directed toward the domain center. The resulting Stokes problem is solved using a conjugate gradient method in combination with a Backward Euler time discretization, see [8]. In this simple test case of the inflated balloon we can derive a stationary analytical solution. As soon as we get to a stationary regime the velocity field and pressure map are:

$$\mathbf{u}(\mathbf{x},t)=\mathbf{0}\quad\forall\mathbf{x}\in\Omega,\quad\forall t\in]0,T[\tag{33}$$

$$p(\mathbf{x},t)=\begin{cases}\kappa(1/R-\pi R), & |\mathbf{x}|\le R\\ -\kappa\pi R, & |\mathbf{x}|>R\end{cases}\quad\forall t\in]0,T[. \tag{34}$$

The parameters used for our simulations are: final time ($T=10^{-1}$), structure density ($\rho_s=1$), fluid density ($\rho_f=1$), fluid viscosity ($\mu=1$), structure stiffness ($\kappa=1$), fluid mesh amplitude ($h_x=1/32$), structure mesh amplitude ($h_s=2\pi R/1024$), time step ($\Delta t=10^{-4}$). Notice that, for the purpose of this paper we are not interested in the effect of inertia terms, being $\rho_s-\rho_f=0$. The interested reader can refer to [2] for a detailed analysis of the case $\rho_s\neq\rho_f$.

In Figure 1(a) we compare the performances of the different finite elements in terms of area conservation. We observe that adding piecewise constant functions to the pressure space the area loss is decreased by five times. As predicted in Section 3.1 the imposition of (28) is effective in reducing the "boundary leakage" effect. A deeper understanding of this result is achieved considering Figure 1(b). Here we plot the L^2-norm of the "real divergence" defined as:

$$\nabla\cdot\mathbf{u}_h=\sum_{j=1}^{df}u_{1j}\frac{\partial\varphi_j}{\partial x}+u_{2j}\frac{\partial\varphi_j}{\partial y}.$$

where φ_j are the basis functions and *df* is the number of degrees of freedom on $K\in\mathcal{T}_h$ for the *Hood–Taylor* scheme. For the *Bercovier–Pironneau* scheme *df* are the degrees of freedom of the single triangle in $\mathcal{T}_{h/2}$. The "real divergence" for the *Hood–Taylor* scheme is piecewise linear, while it is piecewise constant for the *Bercovier–Pironneau* one. Plot 1(b) shows that *Hood–Taylor* scheme is affected by slightly greater values of the "real divergence". This is explaining why the area loss is slightly larger for P_2 finite elements. This result can be at first surprising in the sense that improving the element accuracy provides an overall scheme with slightly more diffusive properties.

Figures 3 and 4 represent the pressure profile at the mid section of the domain for the *Hood–Taylor* and the *Bercovier–Pironneau* schemes, respectively. The numerical and analytical solutions are superimposed. A detailed representation of the Gibbs phenomenon is shown in 3(b), and 4(b). In both cases, the augmented pressure space is effective in reducing the oscillations, resulting in a sharper pressure profile.

Tables 1 and 2 report the convergence analysis for the four finite elements. In the same manner as in [1], augmenting the pressure space is reducing the solution error for both the finite elements. The rate of convergence for *Bercovier–Pironneau* and *Hood–Taylor* elements is comparable, since the discontinuity in the solution provides an upper limit for the achievable accuracy.

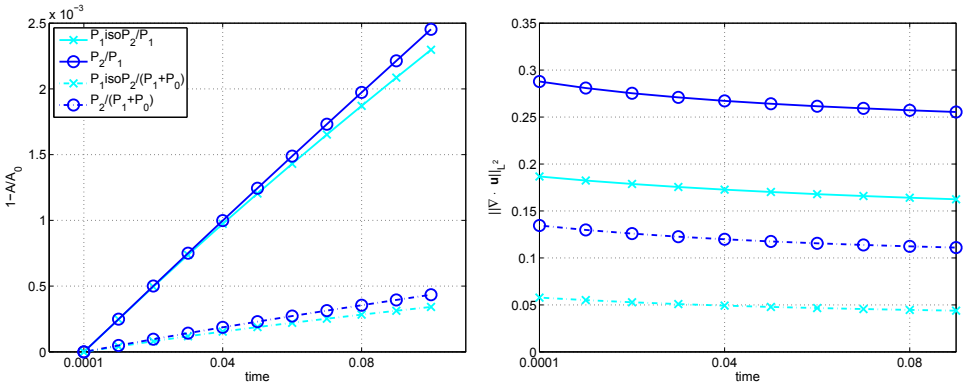

(a) Area loss with respect to time. (b) Real divergence with respect to time.

Figure 1: Boundary leakage and real divergence for solution spaces.

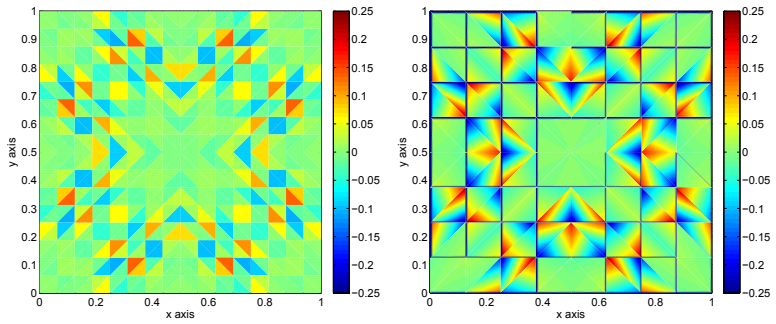

(a) Bercovier Pironneau element. (b) Hood Taylor element.

Figure 2: Real divergence for the augmented spaces.

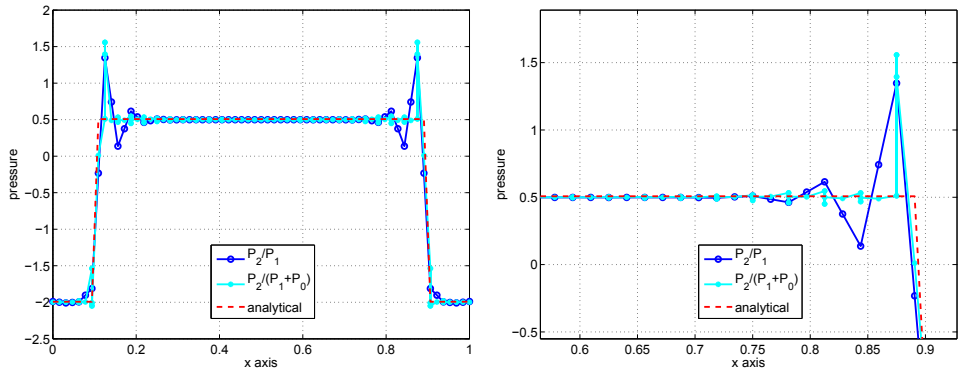

(a) Pressure profile. (b) Pressure detail.

Figure 3: Pressure profile for Hood-Taylor finite element.

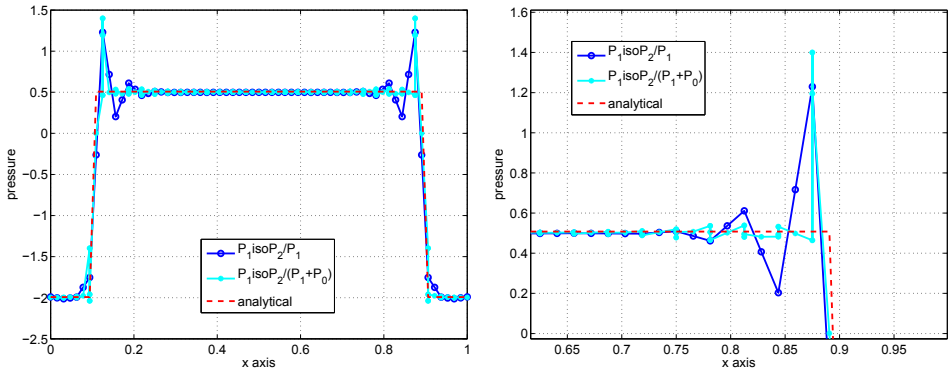

(a) Pressure profile. (b) Pressure detail.

Figure 4: Pressure profile for Bercovier-Pironneau finite element.

$P_1 iso P_2/P_1 + P_0$					
h_x	DOF	$\|\|p_h - p\|\|_{L^2}/\|\|p\|\|_{L^2}$	L^2 rate	$\|\|\mathbf{u}_h - \mathbf{u}\|\|_{L^2}$	L^2 rate
1/8	289	$2.796936 \cdot 10^{-1}$	-	$1.773827 \cdot 10^{-3}$	-
1/16	1084	$1.896726 \cdot 10^{-1}$	0.5603356	$9.032238 \cdot 10^{-4}$	0.9737103
1/32	4225	$1.349056 \cdot 10^{-1}$	0.4915617	$3.291174 \cdot 10^{-4}$	1.456481
1/64	16641	$1.021229 \cdot 10^{-1}$	0.4016440	$1.191034 \cdot 10^{-4}$	1.466388
$P_1 iso P_2/P_1$					
h_x	DOF	$\|\|p_h - p\|\|_{L^2}/\|\|p\|\|_{L^2}$	L^2 rate	$\|\|\mathbf{u}_h - \mathbf{u}\|\|_{L^2}$	L^2 rate
1/8	289	$4.382848 \cdot 10^{-1}$	-	$9.247036 \cdot 10^{-3}$	-
1/16	1084	$3.055532 \cdot 10^{-1}$	0.5204451	$3.031251 \cdot 10^{-3}$	1.609078
1/32	4225	$2.296133 \cdot 10^{-1}$	0.4122172	$1.045616 \cdot 10^{-3}$	1.535560
1/64	16641	$1.715187 \cdot 10^{-1}$	0.4208407	$3.937636 \cdot 10^{-3}$	1.408951

Table 1: Spatial convergence to the reference stationary solution.

$P_2/P_1 + P_0$					
h_x	DOF	$\|\|p_h - p\|\|_{L^2}/\|\|p\|\|_{L^2}$	L^2 rate	$\|\|\mathbf{u}_h - \mathbf{u}\|\|_{L^2}$	L^2 rate
1/8	289	$2.679253 \cdot 10^{-1}$	-	$1.666593 \cdot 10^{-3}$	-
1/16	1084	$1.873964 \cdot 10^{-1}$	0.5157377	$9.165198 \cdot 10^{-4}$	0.8626639
1/32	4225	$1.323534 \cdot 10^{-1}$	0.5016974	$3.115031 \cdot 10^{-4}$	1.556920
1/64	16641	$9.766083 \cdot 10^{-2}$	0.4385436	$1.083690 \cdot 10^{-4}$	1.523295
P_2/P_1					
h_x	DOF	$\|\|p_h - p\|\|_{L^2}/\|\|p\|\|_{L^2}$	L^2 rate	$\|\|\mathbf{u}_h - \mathbf{u}\|\|_{L^2}$	L^2 rate
1/8	289	$3.015382 \cdot 10^{-1}$	-	$8.617810 \cdot 10^{-3}$	-
1/16	1084	$2.277048 \cdot 10^{-1}$	0.4051762	$3.043257 \cdot 10^{-3}$	1.501705
1/32	4225	$1.590665 \cdot 10^{-1}$	0.5175350	$1.030705 \cdot 10^{-3}$	1.561984
1/64	16641	$1.144642 \cdot 10^{-1}$	0.4747342	$3.776420 \cdot 10^{4}$	1.448540

Table 2: Spatial convergence to the reference stationary solution.

5 CONCLUSIONS

At the beginning of this paper we recalled the immersed boundary method in its variational formulation as in [7] and [5]. The key idea is to split the Cauchy stress tensor into two components to be treated in Eulerian and in Lagrangian formulation for the fluid and the structure, respectively.

The main result of this paper is the study of the performances of two families of finite elements whose stability was proved in [1]. Being the solution for the pressure discountinuous, we augmented the pressure space with piecewise constant functions. In Section 3.1 we anticipated two improvements in augmenting the pressure space: better mass conservation, and better oscillations control at the interface. Numerical results show the accomplishment of both these goals. On the other hand we experienced a non-intuitive result for the "real divergence". The *Hood–Taylor* scheme makes the whole IBM algorithm more diffusive than the *Bercovier–Pironneau* one. Considering the "real divergence" it is straightforward to notice that the latter enjoys a more "flexible" shape which is more effective in adjusting the "real divergence" to the structure inclusion (see Figure 2).

Finally, we can conclude that the behavior of both *augmented* elements (*Bercovier–Pironneau* and *Hood–Taylor*) is comparable.

REFERENCES

[1] D. Boffi, N. Cavallini, F. Gardini, and L. Gastaldi. Local mass conservation of stokes finite elements. *Submitted*.

[2] D. Boffi, N. Cavallini, and Gastaldi. Finite element approach to immersed boundary method with different fluid and solid densities. *Submitted*.

[3] D. Boffi and L. Gastaldi. A finite element approach for the immersed boundary method. *Comput. & Structures*, 81(8-11):491–501, 2003. In honour of Klaus-Jürgen Bathe.

[4] D. Boffi, L. Gastaldi, and L. Heltai. A finite element approach to the immersed boundary method. In Scotland Saxe-Coburg Publications, Stirling, editor, *Progress in Engineering Computational Technology, B.H.V. Topping and C.A. Mota Soares Eds.*, pages 271–298, 2004.

[5] D. Boffi, L. Gastaldi, and L. Heltai. Numerical stability of the finite element immersed boundary method. *Math. Models Methods Appl. Sci.*, 17(10):1479–1505, 2007.

[6] D. Boffi, L. Gastaldi, and L. Heltai. On the CFL condition for the finite element immersed boundary method. *Comput. & Structures*, 85(11-14):775–783, 2007.

[7] D. Boffi, L. Gastaldi, L. Heltai, and Charles S. Peskin. On the hyper-elastic formulation of the immersed boundary method. *Comput. Methods Appl. Mech. Engrg.*, 197(25-28):2210–2231, 2008.

[8] R. Glowinski. Finite element methods for incompressible viscous flow. In *Handbook of numerical analysis, Vol. IX*, Handb. Numer. Anal., IX, pages 3–1176. North-Holland, Amsterdam, 2003.

[9] B.E. Griffith. On the volume conservation of the immersed boundary method. *Submitted*.

[10] Boyce E. Griffith, Richard D. Hornung, David M. McQueen, and Charles S. Peskin. An adaptive, formally second order accurate version of the immersed boundary method. *Journal of Computational Physics*, 223(1):10 – 49, 2007.

[11] Boyce E. Griffith and Charles S. Peskin. On the order of accuracy of the immersed boundary method: Higher order convergence rates for sufficiently smooth problems. *Journal of Computational Physics*, 208(1):75 – 105, 2005.

[12] G. Guidoboni, R. Glowinski, N. Cavallini, and S. Canic. Stable loosely-coupled-type algorithm for fluid-structure interaction in blood flow. *J. Comput. Phys.*, 228(18):6916–6937, 2009.

[13] A. Huerta and W. K. Liu. Viscous flow with large free surface motion. *Comput. Methods Appl. Mech. Engrg.*, 69:277–324, 1988.

[14] T. J. R. Hughes, W. K. Liu, and T. K. Zimmermann. Lagrangian-eulerian finite element formulation for incompressible viscous flows. *Comput. Methods Appl. Mech. Engrg.*, 29:329–349, 1981.

[15] P. L. Le Tallec and J. Mouro. Fluid structure interaction with large structural displacements. *Comput. Methods Appl. Mech. Engrg.*, 190:3039–3067, 2001.

[16] C. S. Peskin. The immersed boundary method. In *Acta Numerica 2002*. Cambridge University Press, 2002.

[17] R. Pierre. Local mass conservation and C^0-discretizations of the Stokes problem. *Houston J. Math.*, 20(1):115–127, 1994.

[18] A. Quarteroni, M. Tuveri, and A. Veneziani. Computational vascular fluid dynamics: problems, models and methods. *Comput. Visual Sci.*, 2:163–197, 2000.

[19] D. M. Tidd, R. W. Thatcher, and A. Kaye. The free surface flow of Newtonian and non-Newtonian fluids trapped by surface tension. *Internat. J. Numer. Methods Fluids*, 8(9):1011–1027, 1988.